How Reliable Is DFT in Predicting Relative Energies of Polycyclic Aromatic Hydrocarbon Isomers? Comparison of Functionals from Different Rungs of Jacob's Ladder

Amir Karton*

Density functional theory (DFT) is the only quantum-chemical avenue for calculating thermochemical/kinetic properties of large polycyclic aromatic hydrocarbons (PAHs) such as graphene nanoflakes. Using CCSD(T)/CBS PAH isomerization energies, we find that all generalized gradient approximation (GGA) and meta GGA DFT functionals have severe difficulties in describing isomerization energies in PAHs. The poor performance of these functionals is demonstrated by the following root-mean-square deviations (RMSDs) obtained for a database of $C_{14}H_{10}$ and $C_{18}H_{12}$ isomerization energies. The RMSDs for the GGAs range between 6.0 (BP86-D3) and 23.0 (SOGGA11) and for the meta GGAs they range between 3.5 (MN12-L) and 11.9 (τ-HCTH) kJ mol^{-1}. These functionals (including the dispersion-corrected methods) systematically and significantly underestimate the isomerization energies. A consequence of this behavior is that they all predict that chrysene (rather than triphenylene) is the most stable $C_{18}H_{12}$ isomer. A general improvement in performance is observed along the rungs of Jacob's Ladder; however, only a handful of functionals from rung four give good performance for PAH isomerization energies. These include functionals with high percentages (40–50%) of exact Hartree–Fock exchange such as the hybrid GGA SOGGA11-X (RMSD = 1.7 kJ mol^{-1}) and the hybrid-meta GGA BMK (RMSD = 1.3 kJ mol^{-1}). Alternatively, the inclusion of lower percentages (20–30%) of exact exchange in conjunction with an empirical dispersion correction results in good performance. For example, the hybrid GGA PBE0-D3 attains an RMSD of 1.5 kJ mol^{-1}, and the hybrid-meta GGAs PW6B95-D3 and B1B95-D3 result in RMSDs below 1 kJ mol^{-1}. © 2016 Wiley Periodicals, Inc.

DOI: 10.1002/jcc.24669

Introduction

Polycyclic aromatic hydrocarbons (PAHs) are one of the most important classes of organic compounds. Due to their unique electronic structures and properties they found numerous applications in a variety of industries, for example in organic electronics, semiconductors, dyes, drugs, discotic liquid crystals, and fluorescent/electroluminescent reagents.[1–11] PAHs are also major by-products of incomplete combustion processes and their ubiquitous presence in the environment is of concern due to their carcinogenic and mutagenic potencies.[12,13] Over the past two decades density functional theory (DFT) has become the dominant electronic structure method in materials and quantum chemistry due to its attractive accuracy-to-computational cost ratio. DFT has been extensively used for modeling reactions involving PAHs and calculating their chemical properties (see, e.g., Refs. [14–29]). The ability of DFT to predict of the relative energies of PAHs and to accurately describe potential energy surfaces involving PAHs is of central importance to many of these studies.

The molecular structures of PAHs can have significant effects on their energetic, electronic, and magnetic properties.[30–36] Let us take, for example, the two $C_{14}H_{10}$ PAH isomers: (i) the first ionization potential (IP) of phenanthrene is higher by ~39 kJ mol^{-1} than that of anthracene, (ii) phenanthrene has a larger HOMO–LUMO gap,[31,32] and (iii) while the electronic ring currents in phenanthrene are localized mainly on the terminal rings, in anthracene they are localized mainly on the central ring.[37–39] Similarly, of the five $C_{18}H_{12}$ PAH isomers, triphenylene has the highest IP and the largest HOMO–LUMO gap.[40,41] Ultimately, the different chemical properties of the PAH isomers are a consequence of their topologies,[34,42,43] and therefore are qualitatively well described by Clar's π-sextet rule.[44] According to this empirical rule, the PAH resonance structure with the largest number of disjoint aromatic π-sextets, that is, benzene-like moieties, is the most important one.[45–52] The topological differences between the PAH isomers can also have significant energetic consequences. For example, phenanthrene, which has two isolated sextet rings, is more stable by 25.1 kJ mol^{-1} (*vide infra*) than anthracene, for which only one isolated sextet ring can be drawn (Fig. 1).[31,53–57] Similarly, triphenylene, which has three isolated sextets, is more stable than naphthacene by as much as 53.0 kJ mol^{-1} (Fig. 2).[40,44,50,51] The present manuscript addresses an important question: can DFT functionals from different rungs of Jacob's Ladder adequately describe the energy separations between $C_{14}H_{10}$ and $C_{18}H_{12}$ PAH isomers?

Kohn–Sham DFT is exact in principle, but it involves an unknown exchange-correlation (XC) functional, which has to be approximated.[58] Developing improved approximations for the XC functional is a major ongoing research area.[59–63]

A. Karton
School of Chemistry and Biochemistry, The University of Western Australia, Perth, Western Australia 6009, Australia E-mail: amir.karton@uwa.edu.au

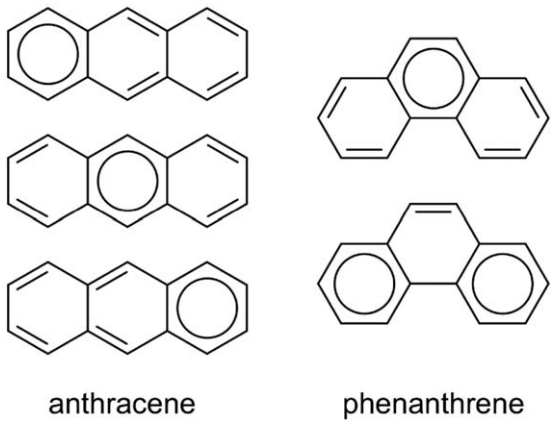

Figure 1. Kekulé resonance structures of the two $C_{14}H_{10}$ isomers. Clar aromatic π-sextets are indicated with a circle.

Despite significant advances in DFT methodology over the past two decades, the various XC approximations often exhibit widely different performances for different chemical properties and systems and do not provide uniform accuracy over a broad range of compounds and thermochemical/kinetic properties. This situation often leads to a practical problem in the application of DFT methods to a given chemical problem. A useful concept that helps DFT users to choose an appropriate DFT functioanal is Perdew's "Jacob's Ladder of DFT."[64] According to this scheme, the various XC functionals are grouped on sequential rungs on a ladder, with each step representing improved accuracy and theoretical complexity. The first rung is the local density approximation, which depends only on the electron density at a given point. The second rung is the generalized gradient approximation (GGA), which uses both the local density and the reduced density gradient. The third rung is the meta generalized gradient approximations (MGGAs), which additionally use the kinetic energy density. The fourth rung is the hybrid-MGGAs, which additionally involve the occupied orbitals. The fifth rung is the double-hybrid functionals, which additionally use the virtual orbitals.[58,65] While, in general, the accuracy of DFT increases as one climbs up the rungs of Jacob's Ladder at present no truly systematic path toward the exact XC functional exists. Thus, the only validation for a given DFT approximation is benchmarking against accurate reference data.[66–69]

It is well established that the performance of DFT can vary for different types of reactions. In particular, the accuracy of a given DFT functional should increase as larger molecular fragments are conserved on the two sides of the reaction, due to an increasing degree of error cancellation between reactants and products.[70–85] The conversion of one PAH isomer into another (e.g., phenanthrene $\rightarrow$ anthracene) conserves the chemical environments on the two sides of the reaction to large extents. In particular, the following features are conserved: the number of (i) sp^2 hybridized carbons, (ii) carbon atoms in each hapticity (i.e., secondary and tertiary), and (iii) aromatic C=C bonds. In addition, in most cases the planarity of the aromatic system is also conserved. The use of transformations in which the chemical environments are largely balanced on the two sides of the reaction, allows us to evaluate the performance of DFT for the calculation of stabilization energies associated with (i) bond length alternations, (ii) local aromaticity (as reflected, for example, from the Clar structures)[34] and (iii) the extent of the overlap between the π-systems of non-neighboring rings (e.g., the overlap between the π-systems of the terminus rings in phenanthrene is larger than that in anthracene).[56]

In the present work, we calculate the relative energies of the $C_{14}H_{10}$ and $C_{18}H_{12}$ isomers at the CCSD(T)/CBS level of theory (coupled cluster with single, double, and quasiperturbative triple excitations extrapolated to the complete basis set limit). We use these benchmark isomerization energies to assess the performance of a wide range of DFT procedures from rungs 2–5 of Jacob's Ladder for the PAH isomerization energies. We find that all of the GGA and MGGA functionals, and many of the hybrid generalized gradient approximation (HGGA) and hybrid-MGGA functionals perform poorly for these PAH isomerization energies and as a consequence fail to predict the lowest-energy $C_{18}H_{12}$ PAH isomer.

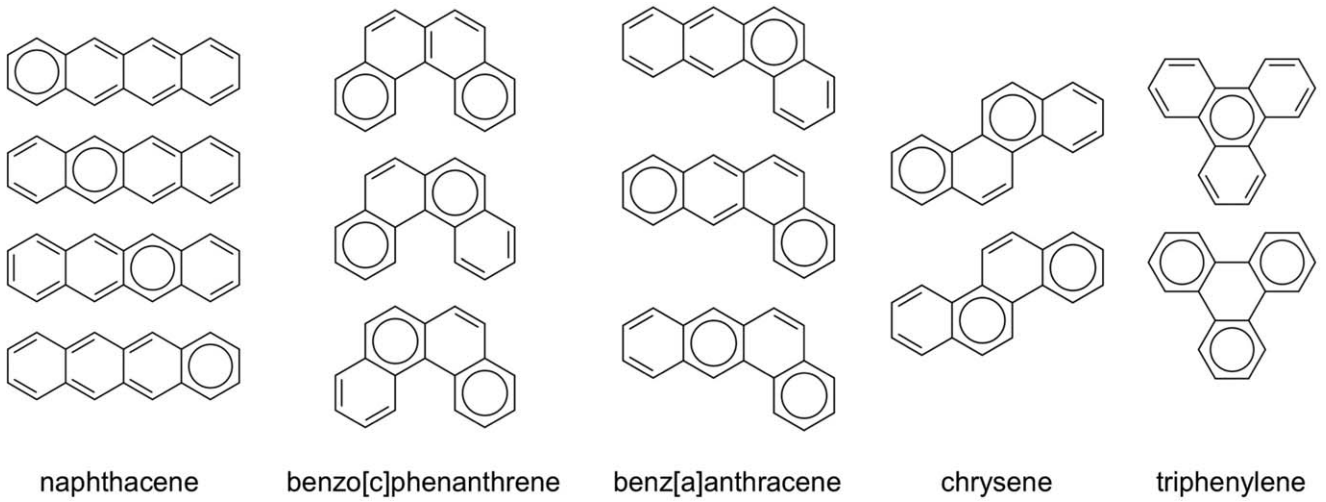

Figure 2. Kekulé resonance structures of the five $C_{18}H_{12}$ isomers. Clar aromatic π-sextets are indicated with a circle.

Computational Methods

To obtain reliable reference isomerization energies for the PAH5 database, calculations have been carried out at the CCSD(T)/CBS level of theory with the Molpro 2012.1 program suite.[86,87] The Hartree–Fock (HF), CCSD, and (T) energies are obtained from W1h theory.[88] W1h theory is a variant of W1 theory,[89] in which the diffuse functions are omitted from carbon. This is of little thermochemical consequence for neutral hydrocarbons, but it does substantially reduce computer resource requirements. In particular, the HF component is extrapolated from the cc-pVTZ and cc-pVQZ basis sets,[90] using the $E(L) = E_\infty + A/L^\alpha$ two-point extrapolation formula, with $\alpha = 5$. The CCSD correlation energy is extrapolated from the same basis sets with an extrapolation exponent of $\alpha = 3.22$, as recommended in Ref. 89. The (T) correlation component is extrapolated from the cc-pVDZ and cc-pVTZ basis sets with $\alpha = 3.22$.[89]

The geometries of all structures have been obtained at the B3LYP-D3/cc-pVTZ level of theory.[91–94] Empirical D3 dispersion corrections[95,96] are included using the Becke−Johnson[97] damping potential as recommended in Ref. 94 (denoted by the suffix -D3). We note that the suffix -D in B97-D and ωB97X-D indicates the original dispersion correction rather than the D3 correction. Harmonic vibrational analyses have been performed to confirm each stationary point as an equilibrium structure (i.e., all real frequencies). All geometry optimizations and frequency calculations were performed using the Gaussian 09 program suite.[98]

As our reference isomerization energies are obtained at the CCSD(T)/CBS level of theory, it is of interest to estimate whether the contributions from post-CCSD(T) excitations are likely to be significant. The percentage of the total atomization energy (TAE) accounted for by parenthetical connected triple excitations, %TAE[(T)], has been shown to be a reliable energy-based diagnostic for the importance of nondynamical correlation effects.[68,99] Table S1 (Supporting Information) gathers the %TAE[(T)] values for the $C_{14}H_{10}$ and $C_{18}H_{12}$ PAH isomers. The %TAE[(T)] values for all the species are lower than 2.5%. It has been found that %TAE[(T)] $\leq$ 5% indicates that post-CCSD(T) contributions to the TAEs should not exceed $\sim$2 kJ mol^{-1}.[100] However, more importantly for the present study, these %TAE[(T)] values indicate that post-CCSD(T) contributions to the isomerization reaction should be negligible.

The DFT XC functionals considered in the present study (ordered by their rung on Jacob's Ladder)[64] are the GGA functionals: BLYP,[91,101] B97-D,[102] HCTH407,[103] PBE,[104] BP86,[101,105] BPW91[101,106]; SOGGA11,[107] N12[108]; the MGGAs: M06-L,[109] TPSS,[110] τ-HCTH,[111] VSXC,[112] BB95,[113] M11-L,[114] MN12-L[115]; the HGGAs: BH&HLYP,[116] B3LYP,[91–93] B3P86,[92,105] B3PW91,[92,106] PBE0,[117] B97-1,[118] B98,[119] X3LYP,[120] SOGGA11-X[121]; the hybrid-MGGAs (HMGGAs): M05,[122] M05-2X,[123] M06,[124] M06-2X,[124] M06-HF,[124] BMK,[125] B1B95,[101,113] TPSSh,[126] τ-HCTHh,[111] and PW6B95[127]; and the DHDFT procedures: B2-PLYP,[128] B2GP-PLYP,[129] B2K-PLYP,[130] B2T-PLYP,[130] DSD-BLYP,[131] DSD-PBEP86,[132,133] PWPB95.[66] We also consider the following range-separated (RS) functionals: CAM-B3LYP,[134] LC-ωPBE,[135] ωB97,[136] ωB97X,[136] ωB97X-D,[137] M11,[138] and MN12-SX.[139]

Table 1. Component breakdown of the benchmark CCSD(T)/CBS isomerization energies in the PAH5 database (reactions 1–5 below, in kJ/mol).

Reaction	ΔHF[a]	ΔCCSD[a]	Δ(T)[b]	ΔCCSD(T)
1	28.9[c]	−2.0[c]	−1.9[c]	25.1[c]
2	−1.8	3.9	0.1	2.1
3	8.9	5.3	−0.1	14.1
4	29.9	−2.7	−2.1	25.0
5	57.5	−0.4	−4.0	53.0

[a] Extrapolated from the cc-pVTZ and cc-pVQZ basis sets. [b] Extrapolated from the cc-pVDZ and cc-pVTZ basis sets. [c] Using larger basis sets in the extrapolations, we obtain: ΔHF/cc-pV{Q,5}Z = 28.96, ΔCCSD/cc-pV{Q,5}Z = −1.93, and Δ(T)/cc-pV{T,Q}Z = −1.91 kJ mol^{-1}. These extrapolations result in ΔCCSD(T) = 25.13 kJ mol^{-1}, which is practically identical to the value obtained from W1h theory.

Results and Discussion

Benchmark isomerization energies for the PAH5 dataset

The PAH5 dataset contains the following five isomerization energies:

$$\text{phenanthrene} \rightarrow \text{anthracene} \quad (1)$$

$$\text{triphenylene} \rightarrow \text{chrysene} \quad (2)$$

$$\text{triphenylene} \rightarrow \text{benz[a]anthracene} \quad (3)$$

$$\text{triphenylene} \rightarrow \text{benzo[c]phenanthrene} \quad (4)$$

$$\text{triphenylene} \rightarrow \text{naphthacene} \quad (5)$$

The component breakdown of the benchmark CCSD(T)/CBS reaction energies are gathered in Table 1. The HF/CBS level of theory overestimates the CCSD(T)/CBS isomerization energies by 3.8 (anthracene), 4.5 (naphthacene), and 4.9 (benzo[c]phenanthrene) kJ mol^{-1}, but underestimates them by 3.9 (chrysene) and 5.2 (benz[a]anthracene) kJ mol^{-1}. Thus, complete neglect of electron correlation does not lead to systematic underestimation or overestimation of the isomerization energies. We note that the HF/CBS level of theory leads to a qualitative error in the triphenylene → chrysene isomerization. Namely, it predicts that the chrysene isomer is more stable than triphenylene by 1.8 kJ mol^{-1}.

The CCSD/CBS level of theory predicts the relative energies of chrysene and benz[a]anthracene practically spot-on, but overestimates the relative energies of anthracene, benzo[c]-phenanthrene, and naphthacene by 1.9, 2.1, and 4.0 kJ mol^{-1}, respectively (Table 1).

For the phenanthrene → anthracene isomerization, we were able to calculate the CCSD(T) energies in conjunction with larger basis sets (i.e., at the W2h level). In particular, the HF and CCSD components are extrapolated from the cc-pV{Q,5}Z basis set pair, and the (T) component is extrapolated from the cc-pV{T,Q}Z basis set pair. These extrapolations indicate that the HF, CCSD, and (T) components from W1h theory are −0.02, −0.06, and +0.04 kJ mol^{-1} away from the infinite basis

Table 2. Statistical analysis for the performance of DFT procedures for the calculation of the isomerization energies in the PAH5 database (in kJ mol^{-1}).[a,b]

Type[c]	Method	RMSD	MAD	MSD	LD[d]
GGA	BLYP	12.7	11.0	−11.0	−22.9 (5)
	BLYP-D3	8.0	7.0	−7.0	−14.4 (5)
	B97-D	8.6	7.6	−7.6	−14.9 (5)
	HCTH407	15.1	13.3	−13.3	−26.3 (5)
	PBE	9.6	8.3	−8.3	−17.3 (5)
	PBE-D3	7.1	6.3	−6.3	−12.8 (5)
	BP86	10.0	8.7	−8.7	−18.1 (5)
	BP86-D3	6.0	5.3	−5.3	−10.7 (5)
	BPW91	10.9	9.5	−9.5	−19.6 (5)
	SOGGA11	23.0	20.9	−20.9	−37.6 (5)
	N12	9.3	8.0	−8.0	−16.9 (5)
MGGA	M06-L	3.6	3.1	−2.5	−6.8 (5)
	TPSS	8.0	6.9	−6.9	−14.6 (5)
	TPSS-D3	4.8	4.2	−4.2	−8.8 (5)
	τ-HCTH	11.9	10.3	−10.3	−21.2 (5)
	VSXC	5.9	5.1	5.1	9.4 (5)
	BB95	9.1	7.9	−7.9	−16.7 (5)
	M11-L	7.8	6.7	−6.7	−13.8 (5)
	MN12-L	3.5	2.9	−2.9	−6.0 (5)
HGGA	BH&HLYP	2.5	2.3	−0.9	−4.0 (3)
	BH&HLYP-D3	2.5	2.1	1.7	4.4 (5)
	B3LYP	7.4	6.2	−6.2	−12.8 (5)
	B3LYP-D3	3.3	2.9	−2.9	−5.8 (5)
	B3P86	4.8	4.0	−4.0	−8.3 (5)
	B3PW91	6.1	5.2	−5.2	−10.6 (5)
	B3PW91-D3	1.8	1.7	−1.7	−3.0 (5)
	PBE0	4.0	3.3	−3.3	−6.6 (5)
	PBE0-D3	1.5	1.3	−1.3	−2.3 (5)
	B97-1	5.8	5.0	−5.0	−10.1 (5)
	B98	6.1	5.2	−5.2	−10.5 (5)
	X3LYP	6.7	5.6	−5.6	−11.5 (5)
	SOGGA11-X	1.7	1.5	−0.5	−2.5 (3)
HMGGA	M05	5.1	4.3	−4.3	−8.7 (5)
	M05-2X	2.6	1.9	1.8	5.0 (5)
	M06	2.7	2.2	−2.1	−4.5 (5)
	M06-2X	2.7	2.1	2.1	5.2 (5)
	M06-HF	7.1	5.4	5.4	14.1 (5)
	BMK	1.3	1.1	−0.2	−1.9 (3)
	BMK-D3	3.0	2.4	2.4	5.6 (5)
	B1B95	2.4	2.1	−1.9	−3.9 (5)
	B1B95-D3	0.9	0.7	0.7	1.7 (5)
	TPSSh	5.9	5.0	−5.0	−10.6 (5)
	τ-HCTHh	6.9	6.0	−6.0	−12.2 (5)
	PW6B95	2.3	2.0	−1.8	−3.6 (5)
	PW6B95-D3	0.7	0.6	−0.4	−1.1 (3)
RS	CAM-B3LYP	1.7	1.6	0.4	2.9 (4)
	CAM-B3LYP-D3	3.0	2.4	2.4	5.4 (5)
	LC-ωPBE	6.8	5.7	5.7	12.5 (5)
	LC-ωPBE-D3	9.3	7.9	7.9	17.3 (5)
	ωB97	8.3	7.2	7.2	15.0 (5)
	ωB97X	6.3	5.5	5.5	11.4 (5)
	ωB97X-D	3.4	2.9	2.9	6.3 (5)
	N12-SX	4.1	3.3	−3.3	−7.0 (5)
	M11	9.4	8.3	8.3	17.0 (5)
	MN12-SX	3.4	2.8	−2.8	−5.4 (5)
DH	B2-PLYP	3.6	3.1	−3.1	−6.3 (5)
	B2-PLYP-D3	1.0	0.9	−0.9	−1.6 (5)
	B2GP-PLYP	1.6	1.3	−1.3	−2.3 (5)
	B2GP-PLYP-D3	0.4	0.4	−0.1	−0.7 (2)
	B2K-PLYP	0.7	0.6	−0.2	−1.1 (2)
	B2K-PLYP-D3	1.0	0.8	0.6	1.8 (5)
	B2T-PLYP	2.3	1.9	−1.9	−3.8 (5)
	DSD-BLYP	1.3	1.1	−1.1	−1.9 (5)
	DSD-PBEP86	1.7	1.5	−1.5	−2.7 (5)
	DSD-PBEP86-D3	0.6	0.5	−0.5	−0.8 (4)
	PWPB95	2.2	1.8	−1.8	−3.7 (5)
	PWPB95-D3	0.9	0.8	−0.8	−1.4 (5)

[a] All DFT calculations were carried out in conjunction with the cc-pVQZ basis set. [b] RMSD = root-mean-square deviation, MAD = mean-absolute deviation, MSD = mean-signed deviation, LD = largest deviation (in absolute value). [c] GGA = generalized gradient approximation, HGGA = hybrid GGA, MGGA = meta GGA, HMGGA = hybrid-meta GGA, RS = range-separated HGGA or HMGGA, DH = double hybrid. [d] The reaction numbers are given in parenthesis (with very few exceptions the largest deviation is obtained for reaction 5).

set limit values. Overall, the difference between the CCSD(T) isomerization energy obtained from W1h and W2h theory is merely −0.04 kJ mol^{-1}.

At the CCSD(T)/CBS limit (from W1h theory), we obtain that phenanthrene is more stable than anthracene by 25.1 kJ mol^{-1}. According to Clar's rule, the outer rings in phenanthrene exhibit larger local aromatic character than the outer rings in anthracene (Fig. 1).[30,55,140] Therefore, the energy difference between the two isomers can be partly explained by Clar's rule. Another factor, which contributes to the greater stability of phenanthrene relative to anthracene, is the more effective overlap between the π-systems of the outer rings in phenanthrene.[56]

In contrast to the relatively large energy separation between the two $C_{14}H_{10}$ isomers, the lowest-energy $C_{18}H_{12}$ isomer (triphenylene) is more stable than chrysene by just 2.1 kJ mol^{-1}. This is consistent with Clar's rule—triphenylene has three isolated sextets, compared with chrysene for which only two isolated sextet rings can be drawn (Fig. 2). The next $C_{18}H_{12}$ isomer, benz[a]anthracene, is less stable than chrysene by 12.0 kJ mol^{-1}. For both isomers resonance structures with two isolated sextet rings can be drawn, however in chrysene there is a more effective overlap between the π-systems of the sextet rings. Benz[c]anthracene is less stable than benz[a]anthracene by 10.9 kJ mol^{-1}. For both isomers resonance structures with two isolated sextet ring can be drawn, thus this energy difference is largely attributed to the non-planar structure of benz[c]anthracene. Naphthacene, for which resonance structures with only one isolated sextet ring can be drawn (Fig. 2), is less stable than benz[c]anthracene by as much as 28.0 kJ mol^{-1}.

Performance of DFT for the isomerization reactions in the PAH5 database

The CCSD(T)/CBS isomerization energies provide a benchmark set of values for the evaluation of the performance of DFT procedures for the calculation of PAH isomerization eneries. For a rigorous comparison with the DFT results, secondary effects that are not explicitly included in the DFT calculations, such as relativity and zero-point vibrational corrections, are not included in the reference values either. Table 2 gives the root-mean-square deviation (RMSD), mean-absolute deviation (MAD), and

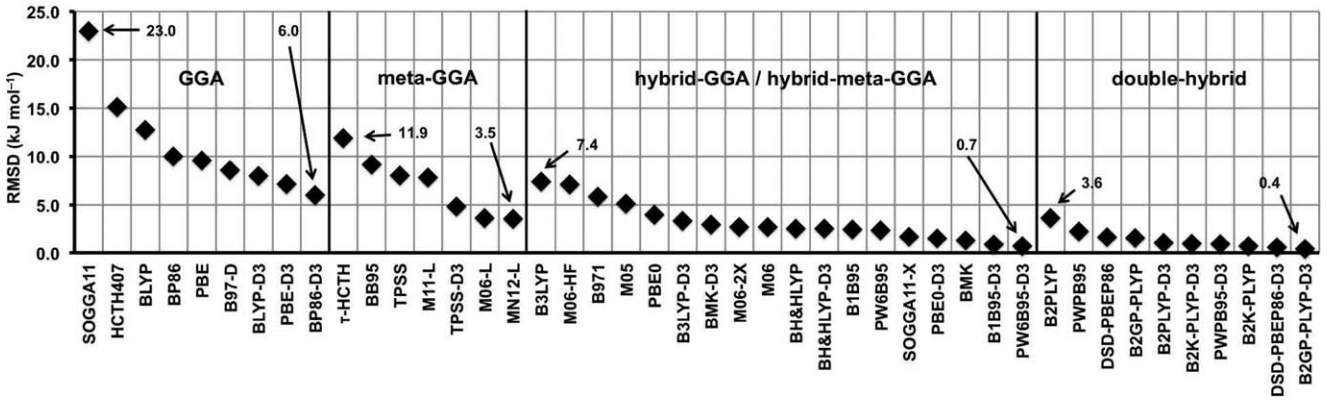

Figure 3. Root-mean-square deviations (RMSDs) for a subset of the DFT procedures over the isomerization energies in the PAH5 database (in kJ mol^{-1}). The RMSDs for all the DFT procedures are given in Table 2 (and in Figure S1 of the Supporting Information).

mean-signed deviation (MSD) from our benchmark W1h results for a series of contemporary DFT functionals (with and without empirical D3 dispersion corrections).

General improvement in performance along the rungs of Jacob's Ladder. Inspection of the error statistics in Table 2 reveals that there is a general improvement in the performance of the DFT functionals along the rungs of Jacob's Ladder. This is illustrated graphically in Figure 3. The RMSDs for the GGA methods (rung 2) spread over a wide range from 23.0 (SOGGA11) to 6.0 (BP86-D3) kJ mol^{-1}. None of the considered GGA methods result in an RMSD below the threshold of "chemical accuracy" (defined here as RMSD $<$ 4 kJ mol^{-1}). The RMSDs for the MGGA methods (rung 3) range between 11.9 (τ-HCTH) and 3.5 (MN12-L) kJ mol^{-1}. Where only the Minnesota functionals MN12-L and M06-L attain RMSDs below the chemical accuracy threshold. The HGGA (rung 3.5) and HMGGA (rung 4) functionals give better performance with RMSDs ranging between 7.4 (B3LYP) and 0.7 (PW6B95-D3) kJ mol^{-1}. Where nearly 60% of the considered methods result in RMSDs below the threshold of chemical accuracy, and about 20% of the methods result in RMSDs smaller than 2 kJ mol^{-1}. Finally, all the considered double-hybrid methods (rung 5) result in RMSDs below the chemical accuracy threshold, with 75% of the functionals attaining RMSDs $<$ 2 kJ mol^{-1}.

Figure 3 reveals another interesting feature, namely that the best-performing functional from each rung are either dispersion corrected or belong to the Minnesota family. For example, the best performing methods of each rung are: (rung 2) PBE-D3 and BP86-D3; (rung 3) M06-L and MN12-L; (rung 4) B1B95-D3 and PW6B95-D3; and (rung 5) DSD-PBEP86-D3 and B2GP-PLYP-D3. The importance of the dispersion corrections will be further discussed in Dispersion corrections section.

GGA and MGGA methods significantly underestimate PAH isomerization energies. Inspection of Table 2 reveals that all the GGA methods systematically underestimate the isomerization energies, as evident from MSD $= -1 \times$ MAD. This is illustrated graphically in Figure 4. The MSDs range from -5.3 (BP86-D3) to -20.9 (SOGGA11) kJ mol^{-1}. The GGA methods show particularly poor performance for the energy difference between triphenylene and naphthacene (reaction 5). The worst performing functional (SOGGA11) underestimates this energy difference by as much as 37.6 kJ mol^{-1}, while the best performing GGA method (BP86-D3) still underestimates this isomerization energy by an appreciable amount of 10.7 kJ mol^{-1}.

The inclusion of the kinetic energy density in the MGGA functionals improves the situation to some extent. However, the MGGAs still systematically underestimate the isomerization energies, with MSDs ranging between -2.5 (M06-L) and -10.3 (τ-HCTH) kJ mol^{-1}. We note that the VSXC functional is a

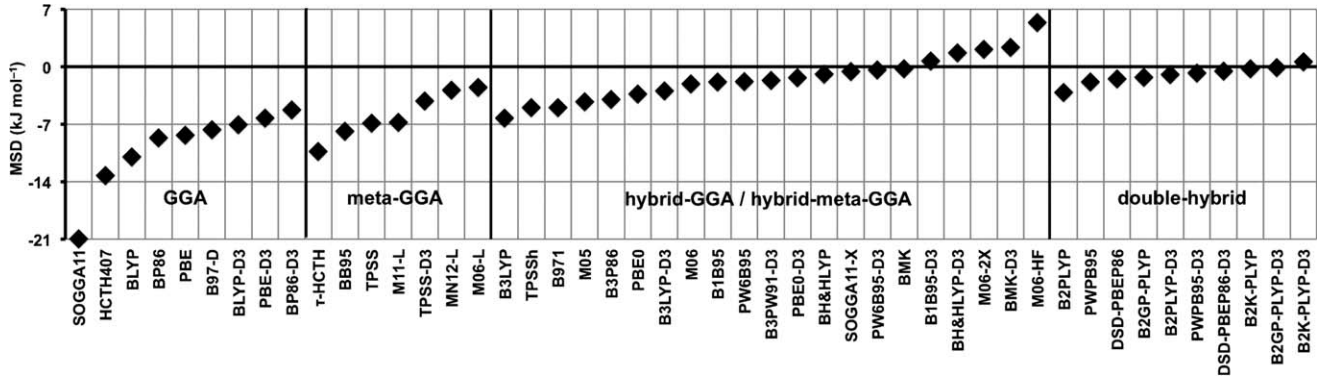

Figure 4. Mean-signed deviations (MSDs) for a subset of the DFT procedures over the isomerization energies in the PAH5 database (in kJ mol^{-1}). The MSDs for all the DFT procedures are given in Table 2 (and in Figure S2 of the Supporting Information).

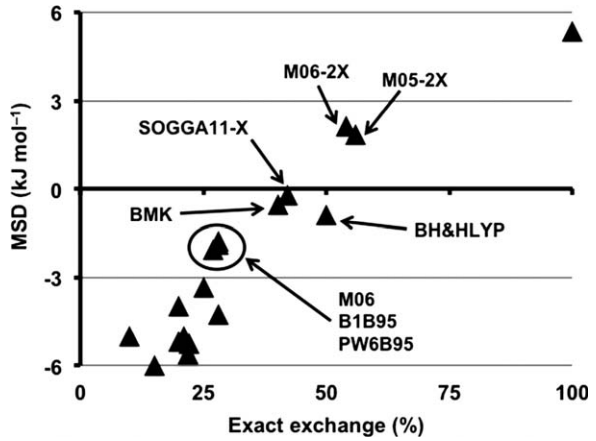

Figure 5. Linear correlation between the MSDs over the PAH5 dataset and the percentage of exact exchange mixing coefficient for the hybrid and hybrid-meta GGA functionals without a dispersion correction. The MSDs are taken from Table 2.

notable exception to this rule as it systematically overestimates the isomerization energies with an MSD of +5.1 kJ mol^{-1}. Again, reaction 5 proves to be very challenging for all the MGGA functionals. This energy separation is underestimated by amounts of 21.2 (τ-HCTH), 14.6 (TPSS), and 13.8 (M11-L). Even the best-performing functionals (MN12-L and M06-L) still underestimate this energy separation by appreciable amounts of 6.0 and 6.8 kJ mol^{-1}, respectively.

Most hybrid and hybrid-MGGAs show good performance. The performance of the 13 HGGA and 13 HMGGA functionals can vary substantially. The RMSDs for the rung 3.5–4 functionals range between 7.4 (B3LYP) and 0.7 (PW6B95-D3) kJ mol^{-1}. The B3LYP and M06-HF functionals are the worst performers with RMSDs $>$ 7 kJ mol^{-1}, while the dispersion-corrected HMGGAs B1B95-D3 and PW6B95-D3 perform exceptionally well with RMSDs $<$ 1 kJ mol^{-1} (Table 2). Inspection of the MSDs in Figure 4 (and Table 2) reveals a general correlation between the amount of exact HF exchange and the functional's MSD. The functionals with the largest MSDs incorporate about 10–25% of exact exchange. For example, hybrid functionals with 20–25% of exact exchange (e.g., B3LYP, B98, B3PW91, B971, B3P86, and PBE0) are associated with MSDs between −6.2 and −3.3 kJ mol^{-1}. Hybrid-MGGA functionals with 10–28% of exact exchange (e.g., τ-HCTHh, TPSSh, M05, M06, B1B95, and PW6B95) are associated with MSDs between −6.0 and −1.8 kJ mol^{-1}. Conversely, functionals with 40–42% of exact exchange (e.g., SOGGA11-X and BMK) are associated with near-zero MSDs, and functionals with 54–100% of exact exchange (e.g., M05-2X, M06-2X, and M06-HF) are associated with positive MSDs.

Figure 5 illustrates the relationship between the percentage of exact HF exchange and the MSDs for the 26 HGGA and HMGGA functionals (for a meaningful comparison between the methods, dispersion-corrected functionals are not included in this plot, dispersion corrections will be discussed separately in Dispersion corrections section). It is evident that functionals with 15–25% of exact exchange are associated with large MSDs ranging between −3 and −6 kJ mol^{-1}. Three functionals with 27–28% of exact exchange give better performance with MSDs of about −2 kJ mol^{-1}, they are: M06, B1B95, and PW6B95. However, the functionals with 40–50% of exact exchange perform significantly better. In particular, the HMGGA BMK (42% of exact exchange) attains a near-zero MSD of −0.2 kJ mol^{-1}, and the HGGA SOGGA11-X (40% of exact exchange) attains an MSD of −0.5 kJ mol^{-1}. We note that the HGGA BH&HLYP with 50% of exact exchange also performs well with an MSD of −0.9 kJ mol^{-1}. Functionals with more than 50% of exact exchange are associated with positive MSDs. In particular, the MSDs for these functionals are: +1.8 (M05-2X), +2.1 (M06-2X), and +5.4 (M06-HF) kJ mol^{-1}.

Finally, it is instructive to compare the performance of the three hybrid functionals B3P86, B3PW91, and B3LYP, which combine Becke's three-parameter exchange functional with different gradient-corrected correlation functionals. These functionals give RMSDs of 4.8, 6.1, and 7.4 kJ mol^{-1}, respectively. Thus, the P86 correlation functional is better than PW91, which in turn is better than the LYP functional. We note that similar trends are observed for the GGAs, i.e., BP86 performs slightly better than BPW91, which in turn performs slightly better than BLYP (Table 2).

Optimal percentage of exact HF exchange. The results of the previous section show that functionals with up to ∼40% of exact HF exchange tend to underestimate the PAH isomerization energies, while functionals with more than ∼50% of exact HF exchange tend to overestimate them. Thus, the optimal percentage of exact HF exchange seems to lie in between ∼40 and 50% (for functionals without a dispersion correction). To investigate this further, we chose two GGAs (PBE and BP86) and two MGGAs (τ-HCTH and TPSS) and we scan the percentage of exact HF exchange. The MSDs and RMSDs over the PAH5 dataset are depicted in Figure 6. It can be seen that for all four functionals the MSD varies linearly with the percentage of exact exchange in the functional form. Low percentages of exact exchange lead to large negative MSDs of up to −10 kJ mol^{-1}, while high percentages of exact exchange lead to large positive MSDs of up to 10 kJ mol^{-1}. The MSD curve crosses the *x*-axis at ∼40–44% of exact HF exchange for all four functionals (consistent with the results in Fig. 5). Figure 6 also shows that at the exact-exchange percentage for which the MSDs are zero, all the functionals result in small RMSDs. In particular, the RMSDs are 1.6 (PBE and BP86), 1.7 (TPSS), and 1.9 (τ-HCTH) kJ mol^{-1} (Fig. 6b). For comparison, the following RMSDs are obtained for the original semi-local functionals: 9.6 (PBE), 10.0 (BP86), 8.0 (TPSS), and 11.9 (τ-HCTH) kJ mol^{-1}, and for the original hybrid and hybrid-meta functionals: 4.0 (PBE0), 5.9 (TPSSh), and 6.9 (τ-HCTHh) kJ mol^{-1}.

Range-separated functionals tend to systematically overestimate PAH isomerization energies. Inspection of the error statistics obtained for the RS methods (Table 2) reveals that, with three exceptions (CAM-B3LYP, N12-SX, and MN12-SX), the RS functionals systematically overestimate the isomerization energies, as evident from MSD = MAD. CAM-B3LYP results in a near-zero MSD of 0.4 kJ mol^{-1}, while N12-SX and MN12-SX

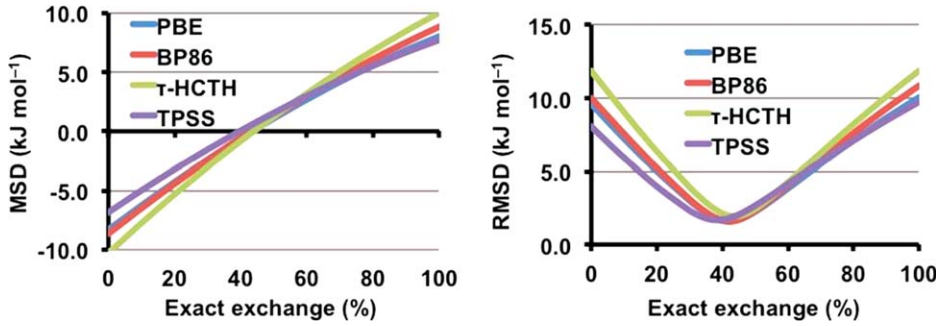

Figure 6. Dependence of the MSD and RMSD over the PAH5 dataset on the exact exchange mixing coefficient for two GGA (blue and red curves) and two meta GGA functionals (green and purple curves). [Color figure can be viewed at wileyonlinelibrary.com]

systematically underestimates the isomerization energies. The different behavior of CAM-B3LYP, N12-SX, and MN12-SX from the other RS functionals may be associated with the percentage of exact HF exchange at long ranges. The functionals that systematically overestimate the isomerization energies (i.e., LC-ωPBE, M11, and the ωB97 family of functionals) include 100% exact HF exchange at long ranges. CAM-B3LYP, conversely, includes 65% HF exchange at long ranges. Whereas N12-SX and MN12-SX, which were developed for solid-state physics and chemical properties, include no HF exchange at long ranges.

Double-hybrid functionals show excellent performance. All the DHDFT methods result in RMSDs below the threshold of chemical accuracy. Remarkably, all of the dispersion-corrected functionals result in RMSDs ≤ 1 kJ mol^{-1}, where B2GP-PLYP-D3 puts in the best performance with an RMSD of merely 0.4 kJ mol^{-1} (Table 2); an MSD of -0.1 kJ mol^{-1} indicates that B2GP-PLYP-D3 is free of systematic bias toward underestimating the PAH isomerization energies.

We will concentrate here on the performance of the non-dispersion-corrected functionals (dispersion corrections will be discussed in the next section). With the exception of B2K-PLYP, all the DHDFT functionals tend to systematically underestimate the PAH isomerizations (as evident from MSD $= -1 \times$ MAD). A closer inspection of the MSDs (Table 2 and Fig. 4) reveals a general correlation between the amounts of exact HF exchange and the MSDs. Functionals with 50–60% of exact HF exchange (B2-PLYP, B2T-PLYP, and PWPB95) results in an MSDs between -1.8 and -3.1; functionals with 65–70% of exact exchange (B2GP-PLYP, DSD-BLYP, and DSD-PBEP86) result in an MSDs between -1.1 and -1.5; while B2K-PLYP (72% of HF exchange) results in a near-zero MSD of -0.2 kJ mol^{-1}. We also note that B2K-PLYP is associated with a large percentage (42%) of MP2-like correlation. Overall, the B2-PLYP method results in the largest RMSD (3.2) and B2K-PLYP results in the smallest RMSD (0.7 kJ mol^{-1}).

Dispersion corrections. As mentioned in General improvement in performance along the rungs of Jacob's Ladder section, the best-performing functionals from each rung of Jacob's Ladder are either dispersion corrected or belong to the Minnesota family (Fig. 3). Table S2 of the Supporting Information gives the contributions of the D3 dispersion corrections to the five isomerization reactions in the PAH5 database. It is evident that dispersion corrections tend to stabilize the energetically more stable isomers to a higher degree (with the exception of benzo[c]phenanthrene). Namely, the magnitude of the dispersion correction (in absolute value) increases in the order: anthracene $<$ phenanthrene for the $C_{14}H_{10}$ isomers, and naphthacene $<$ benz[a]anthracene $<$ chrysene $<$ triphenylene $\sim$ benzo[c]phenanthrene for the $C_{18}H_{12}$ isomers. This trend may be partly explained by the fact that the overlap between the π-systems of the isolated sextet rings is expected to increase in the same order (see Clar's structures in Figs. 1 and 2).

As a result of the above trend in the magnitude of the dispersion corrections, the D3 corrections universally increase the isomerization energies (Table S2, Supporting Information). The one exception to this rule is the triphenylene $\rightarrow$ benzo[c]phenanthrene isomerization, for which dispersion corrections tend to be nil (Supporting Information, Table S2). As most of the DFT procedures from rungs 2–5 of Jacob's Ladder tend to underestimate the PAH isomerization energies (and in many cases by very large amounts), inclusion of the dispersion correction almost always improves the performance of the DFT and DHDFT methods. For the few functionals that tend to overestimate the isomerization energies (most notably the RS functionals CAM-B3LYP and LC-ωPBE), there is no point in including the D3 corrections as they can only increase the deviations. Table 3 gathers the differences in RMSD between the dispersion-corrected and uncorrected DFT functionals (ΔD3 = RMSD(DFT) $-$ RMSD(DFT-D3)). A positive ΔD3 value indicates that the dispersion correction improves the performance of the functional, whereas a negative ΔD3 value indicates deterioration in performance.

Inspection of Table 3 reveals that adding the dispersion D3 corrections for the GGA, MGGA, and HGGA (with 20–25% of HF exchange) methods significantly improve the agreement with the CCSD(T)/CBS reference values. In particular, the RMSDs are reduced by amounts ranging from 2.5 (PBE and PBE0) to 4.8 (BLYP) kJ mol^{-1}. The improvements for the HMGGAs (with 28% of exact exchange) are smaller, ΔD3 being 1.6 kJ mol^{-1} for both B1B95 and PW6B95. The HGGA and HMGGA methods with 40–50% of exact exchange (BH&HLYP and BMK) show excellent performance without the dispersion corrections with small MSDs (-0.9 and -0.2 kJ mol^{-1}, respectively). Thus, there is little point in including dispersion

Table 3. Overview of the performance of various DFT functionals with and without empirical D3 dispersion corrections.[a,b]

Type	Method	ΔD3
GGA	BLYP	4.8
	PBE	2.5
	BP86	4.0
MGGA	TPSS	3.2
HGGA	BH&HLYP	0.0
	B3LYP	4.1
	B3PW91	4.3
	PBE0	2.5
HMGGA	BMK	−1.6
	B1B95	1.6
	PW6B95	1.6
RS	CAM-B3LYP	−1.2
	LC-ωPBE	−2.5
DH	B2PLYP	2.6
	B2GP-PLYP	1.1
	B2K-PLYP	−0.3
	DSD-PBEP86	1.1
	PWPB95	1.3

[a] The tabulated values are ΔD3 = RMSD(DFT) − RMSD(DFT-D3) (in kJ mol^{-1}). [b] Footnotes a–c to Table 2 apply here. RMSD(DFT) and RMSD(DFT-D3) are taken from Table 2.

corrections in these cases. Upon inclusion of the D3 correction to these functionals the isomerization energies are overestimated (with MSDs of +1.7 and +2.4 kJ mol^{-1}, respectively).

Finally, it is worth pointing out that as most DHDFT methods still underestimate the PAH isomerization energies, sizable improvements are obtained upon inclusion of the dispersion corrections. In particular, the RMSDs are reduced by amounts ranging between 1.1 (B2GP-PLYP and DSD-PBEP86) and 2.6 (B2-PLYP) kJ mol^{-1}. A notable exception is B2K-PLYP, for which a near-zero MSD of −0.1 kJ mol^{-1} is obtained; upon inclusion of the D3 correction the MSD becomes +0.6 kJ mol^{-1} and the RMSD increases by 0.3 kJ mol^{-1}.

Practical implications. In this section, we will present two illustrative examples of possible implications of the results presented so far. Namely, we will consider the performance of DFT for the relative energy of isomers separated by either very small or very large energy gaps.

Which DFT Functionals Can Predict the Lowest-Energy $C_{18}H_{12}$ Isomer?. Table 1 shows that the energy separation between the two lowest-energy $C_{18}H_{12}$ isomers is just 2.1 kJ mol^{-1} at the CCSD(T)/CBS level of theory. It is expected that the lowest-energy isomers of larger PAHs will also be separated by small energy gaps. For example, using the best performing DHDFT functional (B2GP-PLYP-D3, Table 2), we find that the three lowest-energy $C_{22}H_{14}$ isomers are separated by less than 4 kJ mol^{-1}. Namely, we obtain the following relative energies in conjunction with the cc-pVQZ basis set: 0.0 (picene), 3.0 (benzo[k]tetraphene, and 3.6 (benzo[m]tetraphene) kJ mol^{-1}. We note that three isolated sextet rings can be drawn for all three isomers (Fig. 7). An important question is: which functionals can predict the lowest-energy PAH isomer in cases where the lowest-energy isomers are separated by small energy gaps (say < 4 kJ mol^{-1}). We will examine this question for the two lowest-energy $C_{18}H_{12}$ isomers, for which we have CCSD(T)/CBS data.

Table S3 of the Supporting Information depicts the energy of chrysene relative to triphenylene obtained by the DFT methods from rungs 2–5 of Jacob's Ladder, while Figure 8 shows these results for a selected subset of methods from rungs 2–4 of Jacob's Ladder. As can be seen, all the GGA methods erroneously predict that chrysene is the lowest-energy $C_{18}H_{12}$ isomer. The GGA fanctionals without a dispersion correction predict that chrysene is more stable than triphenylene by amounts ranging from 11.2 (SOGGA11) to 2.9 (PBE) kJ mol^{-1}. Inclusion of an empirical dispersion correction improves the situation, however, the dispersion-corrected functionals still predict that chrysene is more stable than triphenylene by amounts ranging from 2.6 (B97-D) to 0.3 (BP86-D3) kJ mol^{-1}.

The MGGA methods that do not account for dispersion interactions also predict that chrysene is more stable than triphenylene by considerable amounts, ranging from 4.5 (τ-HCTH) to 2.2 (TPSS) kJ mol^{-1}. TPSS-D3 and M06-L, which were either parameterized for weak interactions or include a dispersion correction, predict that triphenylene and chrysene are essentially isoenergetic (Fig. 8 and Supporting Information Table S3).

Similarly, all the HGGAs that do not account for dispersion interactions via parameterization or a dispersion correction predict that chrysene is more stable than triphenylene by amounts ranging from 2.7 (B3LYP) to 0.7 (BH&HLYP) kJ mol^{-1}. B3LYP-D3 and SOGGA11-X predict that both isomers are essentially isoenergetic. Only three out of the 13 considered HGGAs predict that triphenlyene is the lowest energy isomer. In particular, they predict an energy difference of 0.8 (PBE0-D3), 1.0 (B3PW91-D3), and 1.4 (BH&HLYP-D3) kJ mol^{-1} (cf., an energy difference of 2.1 kJ mol^{-1} at the CCSD(T)/CBS level of theory).

In contrast to most of the DFT methods from rungs 2–3.5 of Jacob's Ladder, most rung 4 functionals predict that triphenlyene is the lowest energy isomer. In particular, only three HMGGAs erroneously predict that chrysene is the most stable $C_{18}H_{12}$ isomer. They are: τ-HCTHh, TPSSh, and M05. Three

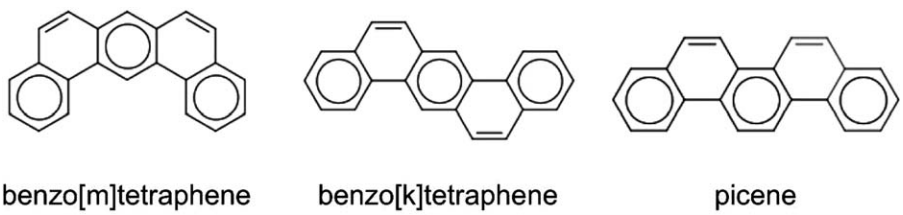

Figure 7. Selected Clar structures for the lowest energy $C_{22}H_{14}$ isomers.

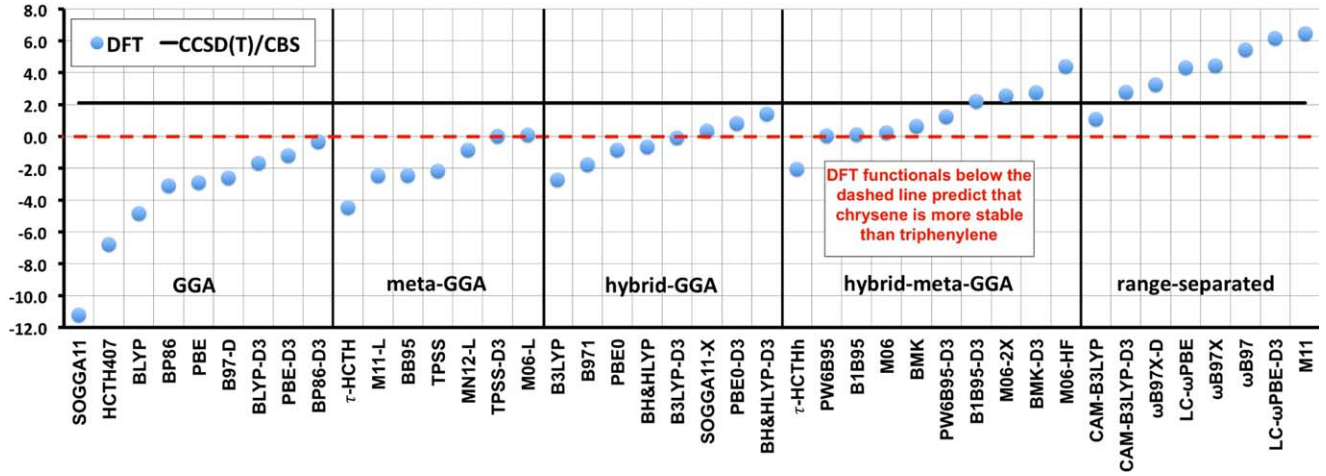

Figure 8. Energy of chrysene relative to the lowest-energy $C_{18}H_{12}$ isomer triphenylene obtained by a subset of DFT methods form rungs 2–4 of Jacob's Ladder (in kJ mol^{-1}). DFT methods below the dashed red line erroneously predict that chrysene is energetically more stable than triphenylene. Figure S3 of the Supporting Information shows these relative energies for all the considered DFT procedures. [Color figure can be viewed at wileyonlinelibrary.com]

methods (PW6B95, B1B95, and M06) predict that triphenylene and chrysene are essentially isoenergetic (Fig. 8 and Supporting Information Table S3), while seven methods predict that triphenylene is more stable by amounts ranging from 0.6 (BMK) to 4.4 (M06-HF) kJ mol^{-1}. The excellent performance of M05-2X and B1B95-D3 should be noted. These two functionals reproduce the CCSD(T) isomerization energy spot-on.

Eight out of the ten considered RS functionas predict that triphenylene is the most stable isomer. However, it should be noted that the RS procedures tend to significantly overestimate the energy gap between the two isomers. In particular, half of the RS functionals predict an energy difference of over twice the CCSD(T)/CBS value; namely, LC-ωPBE, ωB97X, ωB97, LC-ωPBE-D3, and M11 predict that the chrysene isomer lies 4.3–6.5 kJ mol^{-1} above triphenylene.

Finally, we note that with the exception of B2-PLYP, all the DHDFT functionals predict the correct order of stability. However, an empirical dispersion correction is needed to predict the CCSD(T)/CBS energy gap to within 1 kJ mol^{-1}. Of the DHDFT-D3 methods only B2K-PLYP-D3 is able to reproduce the CCSD(T)/CBS isomerization energy to within 0.5 kJ mol^{-1} (Supporting Information Table S3).

Performance of DFT for Isomers Separated by a Large Energy Gap. In the previous subsection, we showed that predicting the correct order of stability of the lowest-lying $C_{18}H_{12}$ isomers is a challenging problem for many DFT methods. Here, we will consider the performance of DFT for relative energies of PAHs that are separated by a large energy gap. We will show that very large errors are obtained for most DFT functionals.

Table S4 of the Supporting Information gives the energy of naphthacene relative to triphenylene obtained by the DFT methods, while Figure 9 shows these results for a subset of methods from rungs 2–4 of Jacob's Ladder. At the CCSD(T)/CBS level of theory, we obtain an isomerization energy of +53.0 kJ mol^{-1} (Table 1). The pure GGA methods severely underestimate this energy difference. GGA methods without a D3 dispersion correction result in very large deviations, ranging from 37.6 (SOGGA11) to 16.9 (N12) kJ mol^{-1}. The dispersion corrected GGAs perform better but still result in large underestimations, ranging between 14.9 (B97-D) and 10.7

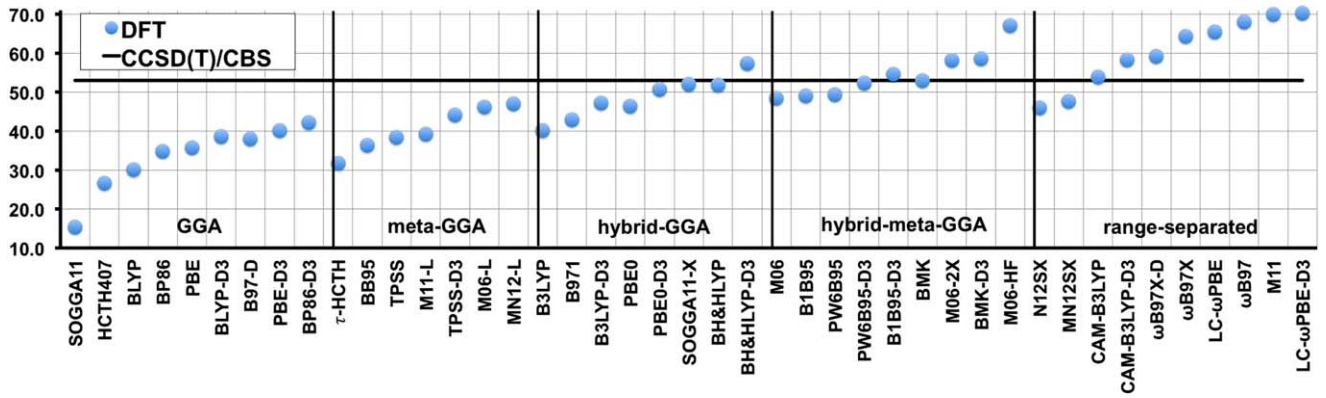

Figure 9. Energy of naphthacene relative to the lowest-energy $C_{18}H_{12}$ isomer triphenylene obtained by a subset of the DFT methods form rungs 2–4 of Jacob's Ladder (in kJ mol^{-1}). Table S4 of the Supporting Information shows these relative energies for all the considered DFT procedures. [Color figure can be viewed at wileyonlinelibrary.com]

(BP86-D3) kJ mol^{-1}. Inclusion of the kinetic energy density in the functional form improves the performance; however, the rung 3 functionals still systematically underestimate the isomerization energy by large amounts of up to 21.2 kJ mol^{-1} (τ-HCTH). The best performing MGGAs result in underestimations of 6.0 (MN12-L) and 6.8 (M06-L) kJ mol^{-1}.

Consistent with the results of the preceding sections, the HGGAs and HMGGAs that involve up to ~30% of exact exchange underestimate the isomerization energies. In particular, eight HGGAs (B3LYP, X3LYP, B3PW91, B98, B971, B3P86, B3LYP-D3, and PBE0) and three HMGGAs (τ-HCTHh, TPSS, and M05) result in sizeable underestimations of 6–13 kJ mol^{-1}. Functionals with ~40–55% of HF exchange overestimate the isomerization energy, where overestimations of over 4 kJ mol^{-1} are obtained for BH&HLYP-D3, M06-2X, BMK-D3, and M05-2X. Note that M06-HF, with 100% of exact exchange, overestimates the isomerization energy by as much as 14.1 kJ mol^{-1}. Finally, we note that two HGGA functionals that give excellent performance are (deviations are given in parenthesis): BH&HLYP (−1.2) and SOGGA11-X (−0.9), and two HMGGA functionals that show exceptional performance are: PW6B95-D3 (−0.6) and BMK (0.0 kJ mol^{-1}).

Most of the RS functionals overestimate the triphenylene–naphthacene isomerization energy by large amounts. In particular, ωB97, ωB97X, LC-ωPBE, LC-ωPBE-D3, and M11 result in overestimations of 11.4–17.3 kJ mol^{-1}. MN12SX and N12SX, conversely, underestimate the isomerization energy by 5.4 and 6.9 kJ mol^{-1}, respectively. These observations are consistent with the results of the previous sections. We note that CAM-B3LYP results in the best performance with a deviation of +0.9 kJ mol^{-1}.

With very few exceptions the DHDFT functiuonals show excellent performance with deviations below the threshold of chemical accuracy. The three best performing DHDFT methods are (deviations are given in parenthesis): DSD-PBEP86-D3 (−0.6), B2K-PLYP (0.0), and B2GP-PLYP-D3 (+0.2 kJ mol^{-1}).

We also evaluated the performance of the various DFT functionals for the energy separation between the lowest- and highest-energy $C_{22}H_{14}$ isomers: picene and pentacene. For these highly symmetric structures, we were able to obtain W1h energies. At the CCSD(T)/CBS level of theory, these isomers are separated by 82.1 kJ mol^{-1}. The performance of the DFT methods for this isomerization energy is discussed in detail in Section S1 of the Supporting Information. Suffice to mention here that both the qualitative and quantitative observations described above remain largely unchanged for the picene–pentacene energy separation.

In summary, it is useful to identify DFT methods that show good performance for both small and large PAH isomerization energies. In this regard, we make the following observations: (i) none of the functionals from rungs 2–3 of Jacob's Ladder can achieve this task, (ii) of the 48 methods from rungs 4–5 of Jacob's Ladder, 21 functionals predict the triphenylene–naphthacene isomerization energy to within chemical accuracy (i.e., to within ±4 kJ mol^{-1}), (iii) of these 21 functionals, only two dispersion-corrected HMGGAs (B1B95-D3 and PW6B95-D3) give acceptable performance for the triphenylene–naphthacene energy separation with deviations smaller than ±1 kJ mol^{-1}, and (iv) all the dispersion-corrected methods from rung 5 of Jacob's Ladder result in deviations smaller than ±1 kJ mol^{-1}.

Conclusions

We have obtained benchmark isomerization energies by means of the high-level W1h composite thermochemistry protocol for the $C_{14}H_{10}$ and $C_{18}H_{12}$ PAH isomers (and some $C_{22}H_{14}$ PAHs). The relative energies of these species are governed by chemical concepts such as local aromaticity (as reflected, e.g., from Clar structures) and the extent of the π-π overlap between non-neighboring rings. These chemical differences between the isomers can have significant energetic consequences. For example, at the CCSD(T)/CBS level of theory the lowest- and highest-energy isomers are separated by 25.1 ($C_{14}H_{10}$), 53.0 ($C_{18}H_{12}$), and 82.1 ($C_{22}H_{14}$) kJ mol^{-1}. Conversely, in some cases the isomers are separated by very small energy gaps. For example, the two lowest-lying $C_{18}H_{12}$ isomers (triphenylene and chrysene) are separated by just 2.1 kJ mol^{-1}.

We use our benchmark PAH isomerization energies (a.k.a. the PAH5 database) to evaluate the performance of a variety of contemporary DFT procedures. We find that the isomerization energies in the PAH5 database are a challenging test for most conventional DFT procedures. With regard to the performance of the conventional DFT procedures (rungs 2–5 of Jacob's Ladder), we make the following observations:

- The GGA functionals (rung 2 of Jacob's Ladder) universally underestimate the isomerization energies. The RMSDs for the functionals without a D3 dispersion correction range between 9.3 (N12) and 23.0 (SOGGA11) kJ mol^{-1}. The functionals with a dispersion correction result in RMSDs between 6.0 (BP86-D3) and 8.6 (B97-D) kJ mol^{-1}. Thus, GGA methods are not recommended for modeling PAH isomerization energies.
- The MGGA functionals (rung 3 of Jacob's Ladder) lead to better performance but still systematically underestimate the isomerization energies. Only the two Minnesota functionals M06-L and MN12-L result in RMSDs below the threshold of chemical accuracy (RMSD = 3.6 and 3.5 kJ mol^{-1}, respectively).
- The HGGA and HMGGA functionals with up to 30% of exact HF exchange tend to systematically underestimate the isomerization energies, in such cases inclusion of a dispersion correction can significantly improve the performance. The best performing functionals from this class are PBE0-D3 and PW6B95-D3 with RMSDs of 1.5 and 0.7 kJ mol^{-1}, respectively.
- The HGGA and HMGGA functionals with 40–55% of exact HF exchange are not biased toward underestimation of the isomerization energies. The best performing functionals from this class are SOGGA11-X and BMK with RMSDs of 1.7 and 1.3 kJ mol^{-1}, respectively. In these cases, inclusion of a dispersion correction tends to lead to a systematic overestimation of the isomerization energies and to poorer overall performance.

- The RS functionals tend to overestimate the isomerization energies. CAM-B3LYP emerges as the best performing method with an RMSD of 1.7 kJ mol^{-1}.
- The double-hybrid procedures (rung 5 of Jacob's Ladder) give excellent performance. The best performing functionals are (RMSDs are given in parenthesis): B2GP-PLYP-D3 (0.4), DSD-PBEP86-D3 (0.6), B2K-PLYP (0.7), and PWPB95-D3 (0.9 kJ mol^{-1}).

The results outlined above mean that many DFT functionals from rungs 2–4 of Jacob's Ladder should be applied with caution for modeling relative energies of PAHs. We demonstrate this in two scenarios, namely, calculating the relative energies of isomers separated by very small or very large energy gaps:

- Predicting the lowest-energy $C_{18}H_{12}$ isomer is a taxing problem for DFT methods from rungs 2–3 of Jacob's Ladder. All of the considered GGA and MGGA functionals erroneously predict that chrysene is the most stable isomer (or isoenergetic with triphenylene). This includes all the dispersion corrected methods. This task is still quite challenging for most HGGAs, where only 3 out of the 13 methods predict the correct stability order (namely, PBE0-D3, B3PW91-D3, and BH&HLYP-D3). We note that these predictions are in contrast to Clar's rule, and illustrate the difficulty that lower-rung DFT methods have in describing the intricate factors governing the stability of PAHs.
- Naphthacene lies 53.0 kJ mol^{-1} above the lowest-energy $C_{18}H_{12}$ isomer triphenylene. Calculating this energy difference proves to be an extremely challenging task for functionals from rungs 2–4. In particular, the GGA methods underestimate this energy gap by amounts ranging from 37.6 (SOGGA11) to 10.7 (BP86-D3) kJ mol^{-1}. The MGGA methods underestimate this energy gap by amounts ranging from 21.2 (τ-HCTH) to 5.9 (MN12-L) kJ mol^{-1}. Only a handful of the rung 4 functionals can reproduce this energy difference to within chemical accuracy. Most notably (deviations are given in paranthesis): PBE0-D3 (−2.2), BH&HLYP (−1.1), SOGGA11-X (−0.9), PW6B95-D3 (−0.6), BMK (0.0), CAM-B3LYP (+1.0), and B1B95-D3 (+1.7 kJ mol^{-1}). Similar observations are obtained for the $C_{22}H_{14}$ isomers pentacene and picene, which are separated by 82.1 kJ mol^{-1}.

In summary, we deem the best performing functionals for modeling PAH isomerization energies, as functionals for which the following three criteria hold: (i) the RMSD for the PAH5 dataset is smaller than 4 kJ mol^{-1}, (ii) they are able to predict the correct lowest-energy $C_{18}H_{12}$ isomer, and (iii) they are able to predict the naphthacene–triphenylene energy separation to within ±4 kJ mol^{-1}. With the exception of MN12-L and M06-L, all the functionals from rungs 2–3 of Jacob's ladder are poor performers based on criterion (i) alone. MN12-L does not comply with criteria (2) and (3), and M06-L does not comply with criterion 3. Thus, none of the functionals from rungs 2–3 are deemed as good performers. The following functionals emerge as best performers from rungs 3.5–4 of Jacob's ladder: three HGGAs (PBE0-D3, B3PW91-D3, and SOGGA11-X), five HMGGAs (BMK, PW6B95, PW6B95-D3, B1B95, and B1B95-D3), and one RS functional (CAM-B3LYP). We note that the above three criteria hold for practically all of the rung 5 functionals, where B2GP-PLYP-D3 emerges as the best performing DHDFT method.

Acknowledgments

We gratefully acknowledge the generous allocation of computing time from the National Computational Infrastructure (NCI) National Facility, and an Australian Research Council (ARC) Discovery Early Career Researcher Award (project number: DE140100311). We would like to thank the reviewers of the manuscript for their valuable comments and suggestions.

Keywords: polycyclic aromatic hydrocarbons · isomerization energies · Clar's rule · density functional theory · W1 theory · CCSD(T)

How to cite this article: A., Karton *J. Comput. Chem.* **2016**, DOI: 10.1002/jcc.24669

Additional Supporting Information may be found in the online version of this article.

[1] L. Zhang, Y. Cao, N. S. Colella, Y. Liang, J. L. Bredas, K. N. Houk, A. L. Briseno, *Acc. Chem. Res.* **2015**, *48*, 500.
[2] A. Narita, X. Y. Wang, X. Feng, K. Müllen, *Chem. Soc. Rev.* **2015**, *44*, 6616.
[3] L. T. Scott, *Chem. Soc. Rev.* **2015**, *44*, 6464.
[4] A. Mateo-Alonso, *Chem. Soc. Rev.* **2014**, *43*, 6311.
[5] X. Feng, V. Marcon, W. Pisula, M. R. Hansen, J. Kirkpatrick, F. Grozema, D. Andrienko, K. Kremer, K. Müllen, *Nat. Mater.* **2009**, *8*, 421.
[6] J. E. Anthony, *Angew. Chem. Int. Ed.* **2008**, *47*, 452.
[7] J. Wu, W. Pisula, K. Müllen, *Chem. Rev.* **2007**, *107*, 718.
[8] J. E. Anthony, *Chem. Rev.* **2006**, *106*, 5028.
[9] M. Bendikov, F. Wudl, D. F. Perepichka, *Chem. Rev.* **2004**, *104*, 4891.
[10] S. Laschat, A. Baro, N. Steinke, F. Giesselmann, C. Hägele, G. Scalia, R. Judele, E. Kapatsina, S. Sauer, A. Schreivogel, *Angew. Chem. Int. Ed.* **2007**, *46*, 4832.
[11] L. Schmidt-Mende, A. Fechtenkötter, K. Müllen, E. Moons, R. H. Friend, J. D. MacKenzie, *Science* **2001**, *293*, 1119.
[12] I. J. Keyte, R. M. Harrisonz, G. Lammel, *Chem. Soc. Rev.* **2013**, *42*, 9333.
[13] L. Vereecken, J. S. Francisco, *Chem. Soc. Rev.* **2012**, *41*, 6259.
[14] P. R. Schreiner, Carbon-rich structures: Computational considerations. In Molecules to Materials; M. Haley, R. Tikwinsky, Eds.; Wiley-VCH, **2006**; pp. 334–382.
[15] S. Cazaux, L. Boschman, N. Rougeau, G. Reitsma, R. Hoekstra, D. Teillet-Billy, S. Morisset, M. Spaans, T. Schlathölter, *Sci. Rep.* **2016**, *6*, 19835.
[16] J. Liu, A. Narita, S. Osella, W. Zhang, D. Schollmeyer, D. Beljonne, X. Feng, K. Müllen, *J. Am. Chem. Soc.* **2016**, *138*, 2602.
[17] W. Zeng, Z. Sun, T. S. Herng, T. P. Gonçalves, T. Y. Gopalakrishna, K. W. Huang, J. Ding, J. Wu, *Angew. Chem. Int. Ed.* **2016**, *55*, 8615.
[18] H. B. Zhang, D. Hou, C. K. Law, X. You, *J. Phys. Chem. A* **2016**, *120*, 683.
[19] J. Dang, M. He, *RSC Adv.* **2016**, *6*, 17345.
[20] F. Xu, X. Shi, Q. Zhang, W. Wang, *Chemosphere* **2016**, *162*, 345.
[21] L. Goerigk, R. Sharma, *Can. J. Chem.* (in press). doi:10.1139/cjc-2016-0290, See: http://www.nrcresearchpress.com/doi/abs/10.1139/cjc-2016-0290#.WCL25twRg5g
[22] F. J. Martín-Martínez, E. H. Fini, M. J. Buehler, *RSC Adv.* **2015**, *5*, 753.
[23] D. Holmes, S. Y. Lee, S. D. Lotz, S. C. Nguyen, G. R. Schaller, R. H. Schmidt-Radde, K. P. C. Vollhardt, *Synthesis* **2015**, *47*, 2038.

[24] M. A. Nazrulla, S. Krishnamurty, K. L. N. Phani, *J. Phys. Chem. C* **2014**, *118*, 23058.
[25] A. Karton, *Chem. Phys. Lett.* **2014**, *614*, 156.
[26] A. Santana, A. M. Popov, E. Bichoutskai, *Chem. Phys. Lett.* **2013**, *557*, 80.
[27] F. Seitz1, A. I. S. Holm, H. Zettergren, H. A. B. Johansson, S. Rosén, H. T. Schmidt, A. Ławicki, J. Rangama, P. Rousseau, M. Capron, R. Maisonny, A. Domaracka, L. Adoui, A. Méry, B. Manil, B. A. Huber, H. Cederquist, *J. Chem. Phys.* **2011**, *135*, 064302.
[28] A. Raj, P. L. W. Man, T. S. Totton, M. Sander, R. A. Shirley, M. Kraft, *Carbon* **2010**, *48*, 319.
[29] R. Sivaramakrishnan, R. S. Tranter, K. Brezinsky, *J. Phys. Chem. A* **2005**, *109*, 1621.
[30] G. Portella, J. Poater, J. M. Bofill, P. Alemany, M. J. Sola, *Org. Chem.* **2005**, *70*, 2509. Erratum, ibid, 2005, 70, 4560.
[31] T. Kato, K. Yoshizawa, K. Hirao, *J. Chem. Phys.* **2002**, *116*, 3420.
[32] R. Dabestani, I. N. Ivanov, *Photochem. Photobiol.* **1999**, *70*, 10.
[33] J. A. N. F. Gomes, R. B. Mallion, *Chem. Rev.* **2001**, *101*, 1349.
[34] T. M. Krygowski, M. K. Cyrański, *Chem. Rev.* **2001**, *101*, 1385.
[35] S. W. Slayden, J. F. Liebman, *Chem. Rev.* **2001**, *101*, 1541.
[36] R. Boschi, E. Clar, W. Schmidt, *J. Chem. Phys.* **1974**, *60*, 4406.
[37] E. Steiner, P. W. Fowler, R. W. A. Havenith, *J. Phys. Chem. A* **2002**, *106*, 7048.
[38] Y. Anusooya, A. Chakrabarti, S. K. Pati, S. Ramasesha, *Int. J. Quantum Chem.* **1998**, *70*, 503.
[39] E. Steiner, P. W. Fowler, *Int. J. Quantum Chem.* **1996**, *60*, 609.
[40] D. Moran, F. Stahl, H. F. Bettinger, H. F. Schaefer, P. v R. Schleyer, *J. Am. Chem. Soc.* **2003**, *125*, 6746.
[41] M. Zander, Polycyclische Aromaten-Kohlenwasserstoff und Fullerene; Teubner: Stuttgart, **1995**.
[42] A. Ciesielski, T. M. Krygowski, M. K. Cyrański, A. T. Balaban, *Phys. Chem. Chem. Phys.* **2011**, *13*, 3737.
[43] A. Ciesielski, T. M. Krygowski, M. K. Cyrański, *J. Chem. Inf. Model.* **2008**, *48*, 1358.
[44] E. Clar, The Aromatic Sextet; Wiley: New York, **1972**.
[45] G. Portella, J. Poater, M. Sola, *J. Phys. Org. Chem.* **2005**, *18*, 785.
[46] A. Misra, D. J. Klein, T. Morikawa, *J. Phys. Chem. A* **2009**, *113*, 1151.
[47] M. Sola, J. *Theor. Comput. Chem.* **2013**, *1*, 1.
[48] M. Sola, *Front. Chem.* **2013**, *1*, 22.
[49] D. Bhattacharya, A. Panda, A. Misra, D. J. Klein, *J. Phys. Chem. A* **2014**, *118*, 4325.
[50] E. Clar, Polycyclic Hydrocarbons; Academic: London, **1964**.
[51] M. Randic, *Chem. Rev.* **2003**, *103*, 3449.
[52] Y. Ruiz-Morales, *J. Phys. Chem. A* **2004**, *108*, 10873.
[53] A. T. Balaban, *Pure Appl. Chem.* **1980**, *52*, 1409.
[54] K. Fukui, *Science* **1982**, *218*, 747.
[55] M. K. Cyranski, B. T. Stepien, T. M. Krygowski, *Tetrahedron* **2000**, *56*, 9663.
[56] J. Poater, R. Visser, M. Sola, F. M. Bickelhaupt, *J. Org. Chem.* **2007**, *72*, 1134.
[57] K. Hemelsoet, V. Van Speybroeck, G. B. Marin, F. De Proft, P. Geerlings, M. Waroquier, *J. Phys. Chem. A* **2004**, *108*, 7281.
[58] A. J. Cohen, P. Mori-Sánchez, W. Yang, *Chem. Rev.* **2012**, *112*, 289.
[59] A. E. Mattsson, *Science* **2002**, *298*, 759.
[60] A. J. Cohen, P. Mori-Sánchez, W. Yang, *Science* **2008**, *321*, 792.
[61] R. Car, *Nat. Chem.* **2016**, *8*, 820.
[62] J. Sun, R. C. Remsing, Y. Zhang, Z. Sun, A. Ruzsinszky, H. Peng, Z. Yang, A. Paul, U. Waghmare, X. Wu, M. L. Klein, J. P. Perdew, *Nat. Chem.* **2016**, *8*, 831.
[63] N. Mardirossian, M. Head-Gordon, *J. Chem. Phys.* **2016**, *144*, 214110.
[64] J. P. Perdew, A. Ruzsinszky, J. Tao, V. N. Staroverov, G. E. Scuseria, G. I. Csonka, *J. Chem. Phys.* **2005**, *123*, 062201.
[65] J. P. Perdew, K. Schmidt, Jacob's ladder of density functional approximations for the exchange-correlation energy. In Density Functional Theory and its Application to Materials; V. Van Doren, C. Van Alsenoy, P. Geerlings, Eds.; AIP Conference Proceedings, Vol. *577*, **2001**; p. 1.
[66] L. Goerigk, S. Grimme, *J. Chem. Theory Comput.* **2010**, *6*, 107.
[67] L. Goerigk, S. Grimme, *J. Chem. Theory Comput.* **2011**, *7*, 291.
[68] A. Karton, S. Daon, J. M. L. Martin, *Chem. Phys. Lett.* **2011**, *510*, 165.
[69] L. Goerigk, A. Karton, J. M. L. Martin, L. Radom, *Phys. Chem. Chem. Phys.* **2013**, *15*, 7028.
[70] S. E. Wheeler, K. N. Houk, P. V. R. Schleyer, W. D. Allen, *J. Am. Chem. Soc.* **2009**, *131*, 2547.
[71] M. D. Wodrich, C. Corminboeuf, S. E. Wheeler, *J. Phys. Chem. A* **2012**, *116*, 3436.
[72] S. E. Wheeler, *WIREs Comput. Mol. Sci.* **2012**, *2*, 204.
[73] A. Karton, D. Gruzman, J. M. L. Martin, *J. Phys. Chem. A* **2009**, *113*, 8434.
[74] R. O. Ramabhadran, K. Raghavachari, *J. Chem. Theory Comput.* **2011**, *7*, 2094.
[75] R. O. Ramabhadran, K. Raghavachari, *J. Phys. Chem. A* **2012**, *116*, 7531.
[76] R. J. O'Reilly, A. Karton, L. Radom, *Int. J. Quantum Chem.* **2012**, *112*, 1862.
[77] E. I. Izgorodina, M. L. Coote, L. Radom, *J. Phys. Chem. A* **2005**, *109*, 7558.
[78] S. Grimme, *Org. Lett.* **2010**, *12*, 4670.
[79] A. Karton, J. M. L. Martin, *Mol. Phys.* **2012**, *110*, 2477.
[80] S. Grimme, *Angew. Chem. Int. Ed.* **2006**, *45*, 4460.
[81] S. Grimme, M. Steinmetz, M. Korth, *J. Org. Chem.* **2007**, *72*, 2118.
[82] M. D. Wodrich, C. Corminboeuf, P. V. R. Schleyer, *Org. Lett.* **2006**, *8*, 3631.
[83] M. D. Wodrich, C. Corminboeuf, P. R. Schreiner, A. A. Fokin, P. V. R. Schleyer, *Org. Lett.* **2006**, *9*, 1851.
[84] P. R. Schreiner, *Angew. Chem. Int. Ed.* **2007**, *46*, 4217.
[85] L. J. Yu, A. Karton, *Chem. Phys.* **2014**, *441*, 166.
[86] H.-J. Werner, P. J. Knowles, F. R. Manby, M. Schütz, P. Celani, G. Knizia, T. Korona, R. Lindh, A. Mitrushenkov, G. Rauhut, T. B. Adler, R. D. Amos, A. Bernhardsson, A. Berning, D. L. Cooper, M. J. O. Deegan, A. J. Dobbyn, F. Eckert, E. Goll, C. Hampel, A. Hesselmann, G. Hetzer, T. Hrenar, G. Jansen, C. Köppl, Y. Liu, A. W. Lloyd, R. A. Mata, A. J. May, S. J. McNicholas, W. Meyer, M. E. Mura, A. Nicklaß, P. Palmieri, K. Pflüger, R. Pitzer, M. Reiher, T. Shiozaki, H. Stoll, Stone A. J., R. Tarroni, T. Thorsteinsson, M. Wang, MOLPRO is a package of ab initio programs. Available at: http:www.molpro.net.
[87] H. J. Werner, P. J. Knowles, G. Knizia, F. R. Manby, M. Schütz, *WIREs Comput. Mol. Sci.* **2012**, *2*, 242.
[88] J. M. L. Martin, S. Parthiban, In Quantum-Mechanical Prediction of Thermochemical Data; J. Cioslowski, Ed.; Kluwer: Dordrecht, Vol. 22, **2001**; p. 31.
[89] J. M. L. Martin, G. Oliveira, *J. Chem. Phys.* **1999**, *111*, 1843.
[90] T. H. Dunning, *J. Chem. Phys.* **1989**, *90*, 1007.
[91] C. Lee, W. Yang, R. G. Parr, *Phys. Rev. B* **1988**, *37*, 785.
[92] A. D. Becke, *J. Chem. Phys.* **1993**, *98*, 5648.
[93] P. J. Stephens, F. J. Devlin, C. F. Chabalowski, M. J. Frisch, *J. Phys. Chem.* **1994**, *98*, 11623.
[94] S. Grimme, S. Ehrlich, L. Goerigk, *J. Comput. Chem.* **2011**, *32*, 1456.
[95] S. Grimme, J. Antony, S. Ehrlich, H. Krieg, *J. Chem. Phys.* **2010**, *132*, 154104.
[96] S. Grimme, *WIREs Comput. Mol. Sci.* **2011**, *1*, 211.
[97] A. D. Becke, E. R. Johnson, *J. Chem. Phys.* **2005**, *123*, 154101.
[98] M. J. Frisch, G. W. Trucks, H. B. Schlegel, G. E. Scuseria, M. A. Robb, J. R. Cheeseman, G. Scalmani, V. Barone, B. Mennucci, G. A. Petersson, H. Nakatsuji, M. Caricato, X. Li, H. P. Hratchian, A. F. Izmaylov, J. Bloino, G. Zheng, J. L. Sonnenberg, M. Hada, M. Ehara, K. Toyota, R. Fukuda, J. Hasegawa, M. Ishida, T. Nakajima, Y. Honda, O. Kitao, H. Nakai, T. Vreven, J. A. Montgomery, Jr., J. E. Peralta, F. Ogliaro, M. Bearpark, J. J. Heyd, E. Brothers, K. N. Kudin, V. N. Staroverov, R. Kobayashi, J. Normand, K. Raghavachari, A. Rendell, J. C. Burant, S. S. Iyengar, J. Tomasi, M. Cossi, N. Rega, N. J. Millam, M. Klene, J. E. Knox, J. B. Cross, V. Bakken, C. Adamo, J. Jaramillo, R. Gomperts, R. E. Stratmann, O. Yazyev, A. J. Austin, R. Cammi, C. Pomelli, J. W. Ochterski, R. L. Martin, K. Morokuma, V. G. Zakrzewski, G. A. Voth, P. Salvador, J. J. Dannenberg, S. Dapprich, A. D. Daniels, Ö. Farkas, J. B. Foresman, J. V. Ortiz, J. Cioslowski, D. J. Fox, Gaussian 09, Revision D.01; Gaussian, Inc.: Wallingford, CT, **2009**.
[99] A. Karton, E. Rabinovich, J. M. L. Martin, B. Ruscic, *J. Chem. Phys.* **2006**, *125*, 144108.
[100] A. Karton, *Wiley Interdiscip. Rev. Comput. Mol. Sci.* **2016**, *6*, 292.
[101] A. D. Becke, *Phys. Rev. A* **1988**, *38*, 3098.
[102] S. Grimme, *J. Comput. Chem.* **2006**, *27*, 1787.
[103] A. D. Boese, N. C. Handy, *J. Chem. Phys.* **2001**, *114*, 5497.
[104] J. P. Perdew, K. Burke, M. Ernzerhof, *Phys. Rev. Lett.* **1996**, *77*, 3865; ibid Phys. Rev. Lett. 1997, 78, 1396.
[105] J. P. Perdew, *Phys. Rev. B* **1986**, *33*, 8822.

[106] J. P. Perdew, J. A. Chevary, S. H. Vosko, K. A. Jackson, M. R. Pederson, D. J. Singh, C. Fiolhais, *Phys. Rev. B* **1992**, *46*, 6671.
[107] R. Peverati, Y. Zhao, D. G. Truhlar, *J. Phys. Chem. Lett.* **2011**, *2*, 1991.
[108] R. Peverati, D. G. Truhlar, *J. Chem. Theory Comput.* **2012**, *8*, 2310.
[109] Y. Zhao, D. G. Truhlar, *J. Chem. Phys.* **2006**, *125*, 194101.
[110] J. M. Tao, J. P. Perdew, V. N. Staroverov, G. E. Scuseria, *Phys. Rev. Lett.* **2003**, *91*, 146401.
[111] A. D. Boese, N. C. Handy, *J. Chem. Phys.* **2002**, *116*, 9559.
[112] T. van Voorhis, G. E. Scuseria, *J. Chem. Phys.* **1998**, *109*, 400.
[113] A. D. Becke, *J. Chem. Phys.* **1996**, *104*, 1040.
[114] R. Peverati, D. G. Truhlar, *J. Phys. Chem. Lett.* **2012**, *3*, 117.
[115] R. Peverati, D. G. Truhlar, *Phys. Chem. Chem. Phys.* **2012**, *10*, 13171.
[116] A. D. Becke, *J. Chem. Phys.* **1993**, *98*, 1372.
[117] C. Adamo, V. Barone, *J. Chem. Phys.* **1999**, *110*, 6158.
[118] F. A. Hamprecht, A. J. Cohen, D. J. Tozer, N. C. Handy, *J. Chem. Phys.* **1998**, *109*, 6264.
[119] H. L. Schmider, A. D. Becke, *J. Chem. Phys.* **1998**, *108*, 9624.
[120] X. Xu, Q. Zhang, R. P. Muller, W. A. Goddard, *J. Chem. Phys.* **2005**, *122*, 014105.
[121] R. Peverati, D. G. Truhlar, *J. Chem. Phys.* **2011**, *135*, 191102.
[122] Y. Zhao, N. E. Schultz, D. G. Truhlar, *J. Chem. Phys.* **2005**, *123*, 161103.
[123] Y. Zhao, N. E. Schultz, D. G. Truhlar, *J. Chem. Theory Comput.* **2006**, *2*, 364.
[124] Y. Zhao, D. G. Truhlar, *Theor. Chem. Acc.* **2008**, *120*, 215.
[125] A. D. Boese, J. M. L. Martin, *J. Chem. Phys.* **2004**, *121*, 3405.
[126] V. N. Staroverov, G. E. Scuseria, J. Tao, J. P. Perdew, *J. Chem. Phys.* **2003**, *119*, 12129.
[127] Y. Zhao, D. G. Truhlar, *J. Phys. Chem. A* **2005**, *109*, 5656.
[128] S. Grimme, *J. Chem. Phys.* **2006**, *124*, 034108.
[129] A. Karton, A. Tarnopolsky, J. F. Lamere, G. C. Schatz, J. M. L. Martin, *J. Phys. Chem. A* **2008**, *112*, 12868.
[130] A. Tarnopolsky, A. Karton, R. Sertchook, D. Vuzman, J. M. L. Martin, *J. Phys. Chem. A* **2008**, *112*, 3.
[131] S. Kozuch, D. Gruzman, J. M. L. Martin, *J. Phys. Chem. C* **2010**, *114*, 20801.
[132] S. Kozuch, J. M. L. Martin, *Phys. Chem. Chem. Phys.* **2011**, *13*, 20104.
[133] S. Kozuch, J. M. L. Martin, J. *Comput. Chem.* **2013**, *34*, 2327.
[134] T. Yanai, D. Tew, N. Handy, *Chem. Phys. Lett.* **2004**, *393*, 51.
[135] O. A. Vydrov, G. E. Scuseria, *J. Chem. Phys.* **2006**, *125*, 34109.
[136] J. D. Chai, M. Head-Gordon, *J. Chem. Phys.* **2008**, *128*, 084106.
[137] J. D. Chai, M. Head-Gordon, *Phys. Chem. Chem. Phys.* **2008**, *10*, 6615.
[138] R. Peverati, D. G. Truhlar, *J. Phys. Chem. Lett.* **2011**, *2*, 2810.
[139] R. Peverati, D. G. Truhlar, *Phys. Chem. Chem. Phys.* **2012**, *14*, 16187.
[140] J. M. Schulman, R. L. Disch, *J. Phys. Chem. A* **1999**, *103*, 6669.

Received: 19 September 2016
Revised: 21 October 2016
Accepted: 27 October 2016
Published online on 00 Month 2016